S. von Alfthan, K. Kaski, A. P. Sutton, Order and structural units in simulations of twist grain boundaries in silicon at absolute zero, Physical Review B 74, 134101 (2006).

Order and structural units in simulations of twist grain boundaries in silicon at absolute zero

S. von Alfthan,[1] K. Kaski,[1] and A. P. Sutton[2]
[1]*Helsinki University of Technology, Laboratory of Computational Engineering, P.O. Box 9203, FIN 02015 HUT, Finland*
[2]*Imperial College London, Department of Physics, Exhibition Road, London SW7 2AZ, United Kingdom*
(Received 22 May 2006; published 3 October 2006)

In contrast to previous results of simulations of the ground-state structures of high-angle twist grain boundaries (GB's) in silicon at absolute zero, in which amorphous intergranular films were found, recent experimental results imply structural order in some high-angle twist boundaries. With a novel protocol for simulating twist GB's, which allows the number of atoms at the boundary to vary, we have found new, lower energy, ordered structures. We have also found structural units common to many of these boundaries, which is further evidence that these boundary structures are not arbitrary or disordered. We give a detailed exposition of the results for five boundaries and conclude that there is structural order present in all of them.

DOI: 10.1103/PhysRevB.74.134101 PACS number(s): 61.72.Mm, 82.20.Wt, 68.35.Ct

I. INTRODUCTION

The possible existence of amorphous intergranular films at grain boundaries (GB's) in elemental solids, especially in network solids like Si, has the potential to affect their thermodynamic, mechanical, and electrical properties very significantly. Tilt GB's have been extensively studied both from experimental and computational points of view.[1–3] There is broad agreement that tilt GB's can be described by the structural unit model[4] (SUM), but in the case of twist GB's the results on GB structures at 0 K are less conclusive. Some earlier simulations have suggested[5,6] that high-angle twist GB's in Si lower their energies by forming disordered amorphous intergranular films even at 0 K. However, recent experimental measurements of the energies of (001) twist GB's in Si (Ref. 7) found cusps at misorientations of $\approx 16°$, 23°, 28°, and 37°, known as $\Sigma 25$, $\Sigma 13$, $\Sigma 17$, and $\Sigma 5$ (001) twist boundaries, respectively. These observations indicate there is some degree of structural order at these misorientations. Recently we have made a thorough investigation of the $\Sigma 5$ boundary and found that there are ordered, low-energy structures for this boundary, which were confirmed by first-principles simulations.[8] Our findings contradicted earlier simulations of twist boundaries,[5,6,9–13] which did not find our low-energy ordered structures and which we attributed to inadequate sampling of configurational phase space.

Here we present a detailed study of the $\Sigma 25$, $\Sigma 13$, $\Sigma 17$, $\Sigma 5$, and $\Sigma 29$ (001) twist boundaries. We find new ordered configurations for all boundaries, but with $\Sigma 29$ showing less order than the other boundaries. We have found the same well-defined structural units in $\Sigma 25$, $\Sigma 13$, and $\Sigma 5$ boundaries and that the energies of these ordered boundaries are significantly lower than those previously published.

The paper is organized as follows. We begin by describing the computational approach[8] we have developed to explore the configurational phase space of twist boundaries. This approach has two new principal features which have enabled us to obtain lower-energy relaxed structures. The results of our simulations are then presented for each twist grain boundary in order of increasing misorientation. The results are discussed in terms of the structural order present in the boundaries, the structural unit model, and they are compared with previous results. Finally we conclude that our computational procedure has produced results not only in better agreement with experiment, but they also call into question the results of previous simulations[5,6] of high-angle twist boundaries in silicon, which concluded that they are amorphous layers in their ground-state configurations at absolute zero.

II. COMPUTATIONAL APPROACH

The first new aspect of our computational protocol is the systematic removal of atoms from the GB. The removal of atoms from twist boundaries generates structures which are not accessible to molecular dynamics (MD) simulation with a constant number of atoms. Let the number of atoms in each layer parallel to the GB contained in one primitive repeat cell of the GB be ν. Then let us suppose that the ground-state configuration does not comprise an integer multiple of ν. In reality this could be achieved by removing atoms from the GB and placing them on the free surface. There is no effective mechanism for doing this in a MD simulation with a constant number of atoms, because atoms removed from the boundary would have to become interstitials in the crystals.

First we create an ideal GB by rotating two Si grains about [001] with respect to each other. The rotation angles are $\phi \approx 16°$, 23°, 28°, 37°, and 44° for the $\Sigma 25$, $\Sigma 13$, $\Sigma 17$, $\Sigma 5$, and $\Sigma 29$ boundaries, respectively. We cut out a supercell containing one primitive cell in the GB plane and 30-Å-thick slabs of crystalline Si on either side. The number of atoms per layer in each primitive cell is $\nu = 25$, 13, 17, 5, and 29 for the $\Sigma 25$, $\Sigma 13$, $\Sigma 17$, $\Sigma 5$, and $\Sigma 29$ boundaries, respectively. The supercell is periodic parallel to the GB and has free surfaces normal to the GB. This defines our reference configuration. One grain can translate rigidly with respect to the other both parallel and perpendicular to the GB plane. We have checked that our results are unaffected by increasing the sizes of the adjoining regions of perfect crystal and that the initial translation state does not influence the relaxed structures. Let ΔN denote the number of atoms removed from this reference configuration. For $1 \leq \Delta N < \nu$, atoms are removed randomly from locations within a 6-Å slab centered on the GB. When $\Delta N = \nu$ we remove an entire (004) atomic layer and translate one grain rigidly by $\frac{1}{4}[001]$ to reinstate

the density of the bulk crystal. For $\nu+1 \leq \Delta N \leq 2\nu-1$ we remove between 1 and $\nu-1$ atoms from the $\Delta N=\nu$ configuration. For each value of ΔN, alternative initial configurations are generated by making different random selections of atoms to be removed. After sufficient annealing $\Delta N=2\nu$ is equivalent to removing two entire (004) layers, which recreates the relaxed structure of the reference configuration. Hence removing 2ν or more atoms should not, in principle, create any new configurations.

Second, we melt the material close to the GB to destroy all memory of the initial configuration by carrying out a 100-ps MD run at 3000 K using the Tersoff III (TS) potential.[14] During this annealing we clamp atoms further away than 10 Å from the GB. The equations of motion are integrated using the Verlet leap frog algorithm[15] with a time step of 1 fs. The temperature is controlled by a Berendsen thermostat.[16]

Third, we quench the system initially to 2000 K and carry out an MD simulation where we attempt to explore all possible low-energy states of the boundary by undertaking several cooling-heating cycles. Our MD simulations are of 60 ns duration with a time step of 2 fs and are performed using the TS potential. During these simulations all atoms are free to move. We follow the evolution of the GB structure by averaging the positions of atoms over a time interval of 300 fs. This averaging removes most of the influence of thermal vibrations in atomic positions. We also calculate the bonding network in the average structures and use it to identify when the structure changes. During the quench the temperature is linearly decreased by 33.3 K/ns. If no new structures are visited in 0.5 ns, then we consider the temperature to be too low to sample phase space efficiently. In this case we try to sample more phase space by increasing the temperature by 1000 K to allow the system to escape the local energy minimum. This quenching schedule results in a sawtoothlike temperature profile. In our simulations such temperature steps occur typically 2–3 times during each run. Averaged configurations generated throughout each simulation are sampled every 100 ps, and we write out structures which have been stable for more than 40 ps. These structures are the starting points of energy minimization to 0 K using conjugate gradients. Each relaxation is deemed to be complete when the fractional change in the total potential energy is less than 10^{-12}. By calculating the GB energy of each relaxed structure we identify the minimum-energy structure of the boundary.

The relaxed configurations obtained with the TS potential were made the starting configurations for further conjugate gradient relaxations and energy evaluations using the Stillinger-Weber (SW) potential.[17] We did this to compare our results with the earlier work using the SW potential.[5,6]

To calculate the energy of each relaxed GB we include as many layers from the GB as required to reach layers where the additional contribution is negligible. This turned out always to be significantly less than 20 Å either side of the GB; thus, we consider our choice of 30-Å perfect crystal regions to be sufficiently large.

In order to identify atoms in the GB we have used a bond orientational order parameter per atom.[18] This criterion is used to evaluate the GB width W and the standard deviations of bond lengths and angles. All atoms within 2.7 Å from each other are considered to be bonded. For each atom we calculate a set of complex numbers

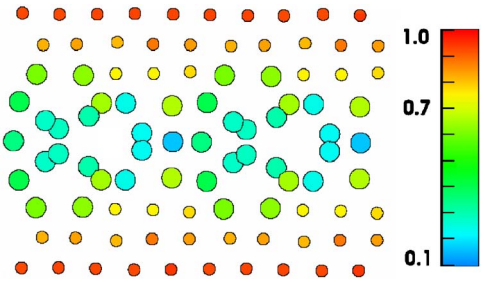

FIG. 1. (Color online) The variation of the order parameter $q(i)$ across the relaxed $\Sigma 5$ GB structure with $\Delta N=7$, viewed sideways along $\langle 310 \rangle$. Large (small) circles show atoms with $q(i)<0.7$ ($q(i)>0.7$). Atoms are colored according to the value of $q(i)$ as indicated by the color bar.

$$\bar{q}_{lm}(i) = \frac{1}{N_b(i)} \sum_{j=1}^{N_b(i)} Y_{lm}(\hat{\mathbf{r}}_{ij}), \tag{1}$$

where $N_b(i)$ is the number of neighbors of atom i, $Y_{lm}(\hat{\mathbf{r}}_{ij})$ are spherical harmonics, and $\hat{\mathbf{r}}_{ij}$ is a unit vector from atom i to a neighbor j. From this we construct a normalized complex vector $\vec{q}_l(i)$ which has $2l+1$ components proportional to $\bar{q}_{lm}(i)$. For atom i we then define the following order parameter:

$$q(i) = \frac{1}{N_b(i)} \sum_{j=1}^{N_b(i)} \vec{q}_6(i) \cdot \vec{q}_6^*(j). \tag{2}$$

By using the addition theorem of spherical harmonics it can be shown that $q(i)$ is always real. It is a measure of the correlation between the angular distribution of the bonds to atom i and the angular distribution of the bonds to i's neighbors. $q(i)$ is unity in a perfect crystal and tends to zero in a completely disordered solid. In Fig. 1 we show the values of $q(i)$ for the relaxed $\Sigma 5$ boundary with $\Delta N=7$. It is seen that $q(i)$ rapidly approaches unity outside the GB region and that it has a mean value of about 0.4 within the GB. This is typical for other relaxed structures. We define atoms in the GB as those having values of $q(i)$ less than 0.7. This region can be seen in Fig. 1 to capture the transitional zone well.

To characterize the shape of a GB we calculate the Voronoi surface between atoms defined to be in the GB and atoms in the crystal grains. This surface describes the shape of the GB region and enables us to calculate the mean width W of the boundary. For some low-angle grain boundaries there are patches of almost perfect crystalline silicon connecting the two grains. Here the local width is zero since the boundary, as defined by the order parameter, does not exist in these areas.

To calculate the standard deviation (σ_b) of the GB bond length distribution we consider all bonds to atoms in the GB. In order to calculate the standard deviation (σ_θ) of the GB bond angles, maximum bond angle (θ_{max}), and minimum bond angle (θ_{min}) we consider angles between all bonds to atoms in the GB.

III. RESULTS

A. Σ25 boundary

The Σ25 boundary has a misorientation of approximately 16° which is the smallest of all boundaries studied here. In each primitive cell of the GB there are 25 atoms per layer, giving 50 possible ΔN values for each primitive cell. In Table I we give structural information for relaxed supercells containing only one primitive cell for all possible ΔN values. For $\Delta N=42-49$ and $0-2$ we find structures containing a regular network of ⟨110⟩ screw dislocations as depicted in Fig. 2. Between these screw dislocations the boundary consists of patches of strained perfect crystal. These boundaries have energies less than 940 mJ/m^2 and exhibit small distortions of bond lengths and angles and very few or no coordination defects. For ΔN values adjacent to this region, approximately $\Delta N=3-11$ and $\Delta N=39-41$, we find structures with a less-well-defined screw dislocation network and smaller patches of perfect crystal. These structures have energies ranging from 933 mJ/m^2 to 1033 mJ/m^2. For other ΔN values we find high energy (up to 1300 mJ/m^2) structures which show a large amount of strain in the bond length and angle distributions and in the existence of four-membered rings. They also have more coordination defects than the low-energy structures and no point-group symmetry, with the exception of $\Delta N=25$, which is a high-energy structure with $p2_122$ space-group symmetry.

The lowest-energy Σ25 structure has a ΔN value of 47 and is depicted in Fig. 2. This boundary has space group $p2$. The screw dislocations have a core structure containing two dimers, one on each side of the boundary plane. At the screw dislocation intersections we find two different core structures which we call units *A* and *B*.

Enlargements of the *A* and *B* structural units are shown in Figs. 3 and 4, respectively. Both units can be characterized using the network of five-membered rings. All atoms which do not participate in a five-membered ring are close to a perfect crystal position of either the upper or lower grain. The five-membered rings form spiral structures which rotate the lattice from the lower grain to the upper one. In unit *A* there are two spirals with two five-membered rings in each of them. In the spiral denoted by the upper arrow in Fig. 3 the upper ring is formed by atoms *a-b-c-h-e-a*, while the lower ring is formed by *d-f-g-b-c-d*. These two rings are connected to each other through two common atoms *b* and *c*. In the spiral denoted by the lower arrow in Fig. 3 the upper ring is formed by atoms *h-j-m-o-l-h*, while the lower ring is formed by *g-l-n-k-i-g*. These two rings are connected to each other through one common atom, *l*. In addition, these spirals are wound around each other so that they have two atoms in common forming a fifth five-membered ring *b-c-h-l-g-b*. This ring is shown with red bonds in the figure. Unit *B* (Fig. 4) consists of one spiral comprising three contiguous five-membered rings, each sharing one atom. The bottom ring shown with blue bonds comprises atoms *d-f-k-m-i-d*. The upper ring shown with red bonds comprises atoms *e-g-j-l-h-e*. The middle ring shown with green bonds comprises atoms *a-b-c-f-e-a* and shares atom *f* with the lower ring and atom *e* with the upper ring. The spirals also displace the position of

TABLE I. Energies (mJ/m^2) of relaxed configurations of Σ25 for $0\leq\Delta N\leq 49$ obtained with the TS potential. The computational repeat cell was equal to the 1×1 primitive cell in the GB plane. Also given are the width *W* in Å of the GB and the number of atoms with a coordination number of 2, 3, 5, and 6 (2,3,5,6) per supercell. σ_b and σ_θ are the standard deviations of the bond lengths and bond angles in the GB (see text). θ_{min} and θ_{max} are the minimum and maximum bond angles in the GB.

ΔN	TS	*W* (Å)	(2,3,5,6)	σ_b (%)	σ_θ (deg)	θ_{min} (deg)	θ_{max} (deg)
0	893	3.6	0,1,1,0	2.1	10.6	76.4	151.6
1	891	3.8	0,1,1,0	2.2	10.4	76.8	156.3
2	876	3.8	0,0,0,0	1.9	9.9	81.7	138.0
3	933	5.0	0,0,0,0	1.8	9.5	82.0	143.1
4	944	4.2	0,0,0,0	2.2	10.0	84.8	146.9
5	960	4.5	0,0,0,0	2.0	9.8	83.0	141.4
6	977	4.0	0,0,2,0	2.4	11.5	72.3	170.6
7	984	4.2	0,0,2,0	2.4	11.2	79.1	173.6
8	991	5.0	0,1,1,0	2.4	10.2	84.7	177.3
9	983	4.7	0,0,0,0	2.4	9.7	85.6	133.0
10	983	4.4	0,0,0,0	2.3	11.0	84.9	176.0
11	1033	4.2	0,0,2,0	2.5	12.2	82.6	174.4
12	1015	4.7	0,0,4,0	2.8	12.1	85.3	176.8
13	1041	6.2	0,0,2,0	2.1	10.4	79.1	173.7
14	1140	5.4	0,1,1,0	2.3	11.2	74.9	173.1
15	1074	4.8	0,0,4,0	2.7	12.4	74.4	172.2
16	1093	4.9	0,0,4,0	2.9	12.5	71.2	173.6
17	1101	4.8	0,1,5,0	2.7	13.4	72.4	174.1
18	1077	4.3	0,0,8,0	3.2	14.7	72.0	172.2
19	1090	4.7	0,0,8,0	3.4	14.1	71.0	171.7
20	1111	5.2	0,0,6,0	3.0	13.6	70.9	170.1
21	1116	5.6	0,0,10,0	3.5	13.9	58.4	166.8
22	1176	7.3	0,1,5,0	2.5	12.0	71.6	173.9
23	1170	5.3	0,0,10,0	3.2	15.0	70.6	175.9
24	1254	7.2	0,2,4,0	2.5	11.0	72.4	176.1
25	1205	5.8	0,0,8,0	3.1	12.9	72.6	166.2
26	1274	6.2	0,0,6,0	2.4	13.0	72.5	163.2
27	1217	5.2	0,0,2,0	2.4	11.1	61.4	165.7
28	1290	5.3	0,1,1,0	2.3	10.2	76.2	157.4
29	1279	6.2	0,1,3,0	2.2	11.1	74.8	165.1
30	1251	6.2	0,0,6,0	2.1	11.8	71.3	176.6
31	1278	6.8	0,0,2,0	1.9	10.5	72.5	160.2
32	1196	4.8	0,0,4,0	2.3	12.0	72.7	174.1
33	1183	4.5	0,0,2,0	2.1	10.8	74.8	175.9
34	1173	4.4	0,0,2,1	2.3	12.3	71.5	176.2
35	1168	5.3	0,0,0,0	1.9	9.7	80.4	137.7
36	1071	4.8	0,0,2,0	1.8	10.6	74.9	155.2
37	1057	4.5	0,0,2,0	1.8	10.9	75.4	172.4
38	1061	5.1	0,0,2,0	2.0	10.5	77.2	173.2
39	1005	4.4	0,0,0,0	1.8	9.4	80.1	136.4
40	995	4.4	0,1,1,0	1.9	10.8	74.4	166.3
41	969	4.9	0,0,2,0	1.9	10.5	61.9	153.5

TABLE I. (*Continued.*)

ΔN	TS	W (Å)	(2,3,5,6)	σ_b (%)	σ_θ (deg)	θ_{min} (deg)	θ_{max} (deg)
42	937	3.9	0,0,2,0	1.9	10.7	72.5	151.1
43	886	3.8	0,0,0,0	1.5	9.4	79.4	132.5
44	913	3.9	0,0,0,1	2.4	10.9	73.4	170.4
45	890	3.9	0,0,2,0	2.0	10.7	71.1	157.9
46	875	4.1	0,0,2,0	2.1	10.5	71.5	158.7
47	836	3.6	0,0,0,0	1.5	9.4	80.0	135.7
48	852	3.9	0,0,0,0	1.8	9.4	80.4	141.2
49	868	3.6	0,0,0,0	1.8	10.3	84.1	140.9

the interface along the normal to the interface. In the *A* unit the interface is shifted downwards by 2.6 Å going from left to right in Fig. 3. In the other direction the interface is not shifted. For the *B* unit the interface is shifted downwards by 2.6 Å when going from left to right in Fig. 4. Again the interface is not shifted in the other direction. For Σ25 and $\Delta N=43$ one can form a boundary with only *A* units in the intersections. There is an energy penalty associated with this boundary; some of the screw dislocations have higher energy cores to accommodate having only *A* units in the boundary.

B. Σ13 boundary

The Σ13 boundary has a misorientation of approximately 23°, and in each primitive cell in the GB plane there are 13 atoms per layer, giving 26 possible values of ΔN per cell. In Table II we list structural information for supercells containing only one primitive cell in the GB plane. Σ13 is similar to

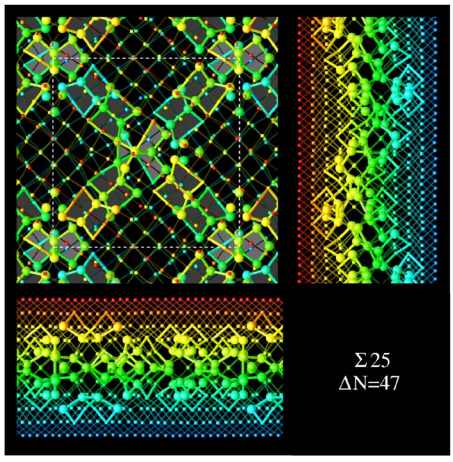

FIG. 2. (Color online) The color of atoms and bonds indicates the position perpendicular to the boundary; blue (red) atoms or bonds are farther from (closer to) the viewer. The larger atoms are defined to be in the GB, and the thicker bonds are bonds forming five-membered rings. We have indicated structural units in the plan view by shading the five-membered rings within them. Structural units in the cores of screw dislocation are shaded darker gray, and *A* and *B* units at the screw dislocation intersections are shaded lighter gray.

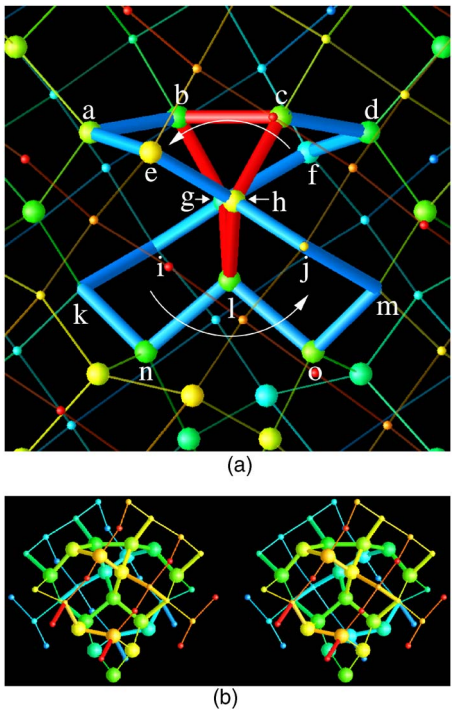

FIG. 3. (Color online) The *A* structural unit, found at some screw dislocation intersections. In the upper figure atoms within five-membered rings are labeled. For clarity one five-membered ring is shown with red bonds and the remaining bonds in five-membered rings are blue. The arrows indicate the sense of the spirals formed by the five-membered rings. In the lower figure the structure is shown as a stereo pair. See caption to Fig. 2.

Σ25 in that there are low-energy structures ($\Delta N=21-25$ and $\Delta N=0$) consisting of networks of ⟨110⟩ screw dislocations and high-energy boundaries ($\Delta N=1-20$), which have more disordered structures. We also find similar structural units in the screw dislocation intersections to those found in Σ25 boundary. Again the low-energy structure have energies in the range of 850–1000 mJ/m^2 while the high-energy boundaries have boundary energies approaching 1300 mJ/m^2. The misorientation is larger than for Σ25, and thus the size of the patch of distorted perfect crystal is smaller and the core of the screw dislocation contains only one pair of dimers between each intersection.

When the supercell comprises one primitive cell in the GB plane the lowest- and next-lowest-energy structures correspond to $\Delta N=21$ and $\Delta N=25$, with energies of 866 and 905 mJ/m^2, respectively. For $\Delta N=21$ both dislocation intersections are *A* units while for $\Delta N=25$ both intersections are *B* units (Fig. 5). In simulations where the supercell comprises one primitive cell we have not found structures with one *A* and one *B* unit. The $\Delta N=22$ and $\Delta N=23$ structures consist of an *A* unit in one of the intersections and one intersection with more disordered characteristics. The $\Delta N=24$ structure consists of a *B* unit in one of the intersections and one intersection with some resemblance to a *B* unit. By increasing the size of the computational cell so that it comprised 2×2 primitive cells we have found several structures containing both *A* and *B* units (Fig. 6 and Table III). Here the energy increases as the fraction of *A* units in the boundary goes

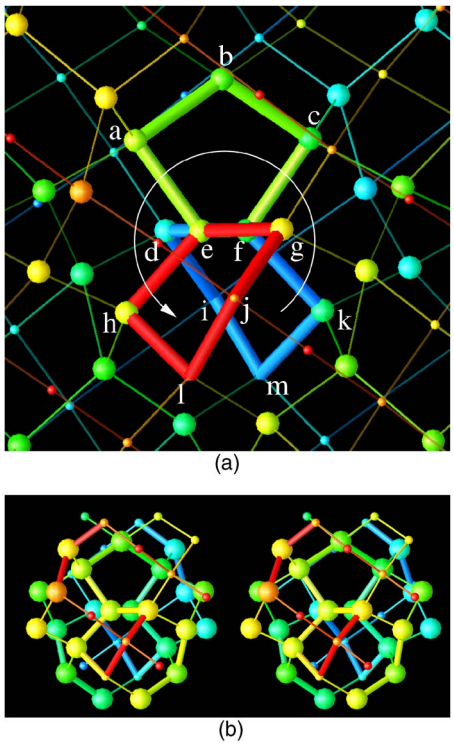

FIG. 4. (Color online) The *B* structural unit, found at some screw dislocation intersections. In the upper figure atoms within five-membered rings are labeled. For clarity one five-membered ring is shown in red, another in green, and the third in blue. The arrow indicates the sense of the spiral formed by these three five-membered rings. In the lower figure the structure is shown as a stereo pair. See caption to Fig. 2.

down. For $\Delta N=21$ with the supercell comprising 2×2 primitive cells we obtain a lower energy (858 mJ/m^2) than that obtained with a computational supercell comprising one primitive cell (866 mJ/m^2).

Each *A* unit in the computational supercell comprising one primitive cell with $\Delta N=21$ is rotated by 180° around [001] relative to its neighbors. This produces a corrugated profile when one looks at the boundary from one side (Fig. 7) because the units raise and lower the interface periodically. We may characterize this interface as $\uparrow\downarrow$ where the arrows signify upward and downward displacement of the location of the interface. In the case of the 2×2 computational supercell the interface is $\uparrow\uparrow\downarrow\downarrow$, which has a lower energy than $\uparrow\downarrow\uparrow\downarrow$. In a macroscopic boundary the interface is free to form any combination of $\uparrow$ and $\downarrow$ but $\cdots\uparrow\downarrow\cdots$ has an energy penalty of $\approx$11 pJ/m compared with $\cdots\uparrow\uparrow\cdots$ or $\cdots\downarrow\downarrow\cdots$. We have calculated one boundary with 4×4 primitive cells. There the boundary did not adopt the lowest-energy state of $\uparrow\uparrow\uparrow\uparrow\downarrow\downarrow\downarrow\downarrow$ but instead formed a $\uparrow\uparrow\uparrow\downarrow\uparrow\downarrow\downarrow\downarrow$ boundary. In this case we believe that the quench did not find the global minimum but a local minimum due the difficulty in finding global minima in larger boundaries.

C. Σ17 boundary

The Σ17 boundary has a misorientation of approximately 28°, and in each primitive cell in the GB plane there are 17 atoms per atomic layer, giving 34 unique ΔN values per cell. In Table IV we give structural information for supercells containing 1×1 primitive cells in the GB plane. For $\Delta N=32$, 33 and $\Delta N=0$ we find low-energy structures with GB energies in the range of 1009–1037 mJ/m^2 and small strain reflected in the bond angle and length distributions. Among the structures with energies up to 1200 mJ/m^2 we have several structures, $\Delta N=12-14$, which belong to space group $p2$. There is also a range of structures, $\Delta N=26-31$, containing one *B* unit. Among the high-energy boundaries there are also several structures $\Delta N=15-21$, which possess no symmetries, are wider, and have more defects and wider bond-angle distributions.

The two lowest-energy 1×1 structures are found with $\Delta N=32$ and $\Delta N=0$ and are depicted in Fig. 8. These structures are defect free but $\Delta N=0$ has two four-membered rings per primitive cell while $\Delta N=32$ has four. The Σ17 boundary is different from Σ25 and Σ13 boundaries in that there is no obvious indication of the ⟨110⟩ screw dislocation network. $\Delta N=0$, which is the second lowest-energy structure, has space group $p2_122$. The lowest-energy structure, however, has less symmetry, with space group $p2_1$. The energy difference between these structures is small, of the order of 1%. In

TABLE II. Relaxed structures of Σ13 for $0\leq\Delta N\leq25$. For notation see caption to Table I.

ΔN	TS	W (Å)	(2,3,5,6)	σ_b (%)	σ_θ (deg)	θ_{min} (deg)	θ_{max} (deg)
0	945	6.1	0,0,0,0	1.9	8.8	91.7	140.2
1	1031	5.5	0,1,1,0	2.4	10.0	76.2	158.3
2	1066	5.7	0,0,2,0	2.4	10.5	79.2	163.2
3	1089	5.4	0,1,1,0	2.3	11.2	77.5	159.2
4	1094	5.2	0,0,2,0	2.7	12.4	77.9	174.9
5	1114	5.5	0,0,4,0	2.9	12.7	72.0	169.3
6	1168	4.7	0,0,2,0	3.2	13.6	71.0	177.8
7	1152	8.0	0,0,0,0	2.0	9.5	64.7	149.0
8	1165	6.0	0,0,2,0	2.7	12.5	80.5	175.8
9	1147	5.3	0,0,0,0	1.9	13.1	85.9	160.8
10	1117	5.8	0,0,0,0	1.7	11.7	83.6	163.8
11	1195	5.7	0,0,4,0	3.0	14.9	72.1	175.4
12	1207	5.7	0,0,6,0	3.3	15.9	70.9	177.3
13	1245	6.4	0,0,2,0	2.3	11.7	82.0	162.7
14	1291	7.5	0,0,2,0	2.3	11.0	70.5	169.4
15	1281	5.0	0,0,2,0	2.2	11.7	74.5	160.8
16	1236	5.0	0,0,4,0	2.6	13.0	59.5	168.7
17	1165	4.6	0,0,0,0	1.9	10.1	66.6	133.5
18	1179	5.0	0,0,2,0	2.6	12.4	62.1	162.1
19	1097	5.1	0,0,2,0	2.3	11.6	62.5	156.8
20	1008	4.8	0,0,4,0	1.7	11.9	74.0	167.2
21	866	4.3	0,0,0,0	1.2	9.1	83.6	129.6
22	944	4.9	0,0,0,1	2.8	11.4	73.1	170.8
23	984	4.9	0,0,2,0	2.6	11.3	71.8	173.6
24	961	6.2	0,2,0,0	1.6	9.1	79.4	145.6
25	905	5.5	0,0,0,0	1.6	8.8	87.8	135.9

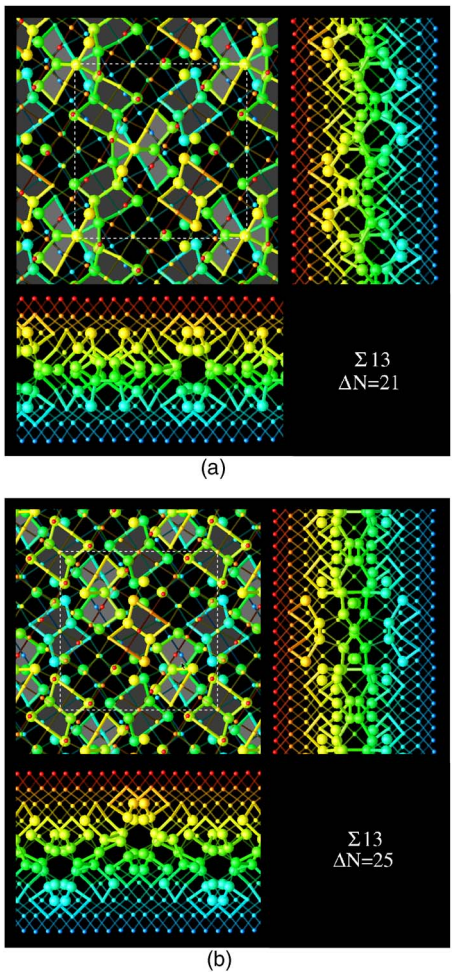

FIG. 5. (Color online) Σ13 boundaries where each simulation supercell contained one primitive cell in the GB plane and the number of atoms removed, ΔN, is 21 in the top figure and 25 in the bottom figure. See caption to Fig. 2.

$\Delta N=0$ there is a row of structural units which consists of four five-membered rings and one four-membered ring resembling a cross in the plan view (see Fig. 9). The five-membered rings are *j-e-c-g-k-j*, *a-b-d-f-c-a*, *p-o-n-f-l-p*, and *h-i-m-l-g-h*. These rings are arranged such that each bond in the four-membered ring *f-c-g-l-f* is also a bond of one of the five-membered rings. In this work we will refer to this structure as the *C* unit.

We have also calculated the minimum energy structure for supercells comprising 2×2 primitive cells. In Table V we give structural information for these boundaries. Here there are 136 possible ΔN values ranging from 0 to 33.75. Since ΔN is the number of atoms removed per primitive cell, it can have fractional values in supercells comprising multiple primitive cells. Owing to computational constraints we have calculated 2×2 cells only for $\Delta N=31-33.5$ and $\Delta N=0$, which includes the ΔN values for the low-energy structures obtained with 1×1 cells. We have found two different structures with an energy of 1007 mJ/m^2 for $\Delta N=31.5$ (Fig. 10) and $\Delta N=32.5$ (Fig. 11). These structures do not exhibit point-group symmetry or any indication of the screw dislocation network. Upon closer examination we notice that

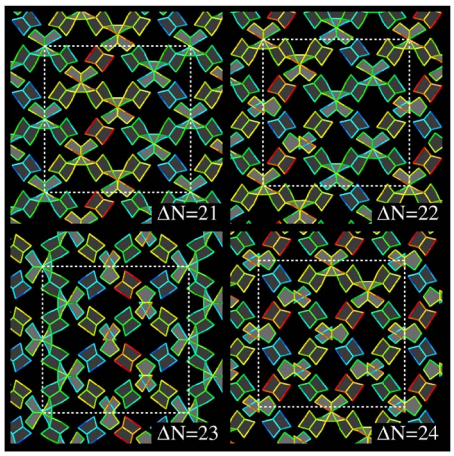

FIG. 6. (Color online) Σ13 boundaries where each simulation supercell contained 2×2 primitive cells in the GB plane. In each case the value of ΔN signifies the number of atoms removed per primitive cell. The size of the supercell is indicated by a white dashed boxes. See caption to Fig. 2. Bonds in only five-membered rings are shown to highlight the structural units.

there is some degree of order evidenced by the structural units present. For $\Delta N=31.5$ we find there are one *A* unit, two *B* units, and two *C* units per computational supercell. For $\Delta N=32.5$ we find that there are six *B* units and one *C* unit per supercell. It appears that other parts of the interface may not be associated with order in terms of symmetry, structural units, or small strain.

D. Σ5 boundary

The Σ5 boundary has a misorientation of approximately 37° and only five atoms per primitive cell in the GB plane, thus making it the smallest of all boundaries studied here. In Table VI we present the relaxed energies and characterizations of the structure for computational supercells comprising one primitive cell in the GB plane. There are two low-energy structures $\Delta N=2$ and 7, and they show no coordination defects. In addition, the two lowest-energy configurations also show the smallest values of σ_b, both of which are significantly less than 2%, and σ_θ, which are about 9°. The highest-energy configuration ($\Delta N=5$) has the largest number (4) of undercoordinated atoms in each primitive cell and among the highest values of σ_b and σ_θ. The lowest-

TABLE III. Relaxed structures of Σ13 with the computational cell comprising $2\times2=4$ primitive cells for $21\leq\Delta N\leq25$. A is the fraction of screw dislocation intersections comprising *A* units, the remainder comprising *B* units. See caption to Table I for notation.

ΔN	TS	A (%)	W (Å)	σ_b (%)	σ_θ (deg)	θ_{min} (deg)	θ_{max} (deg)
21	858	100	4.6	1.2	8.9	82.6	129.7
22	870	75	5.0	1.3	8.8	82.5	136.6
23	876	50	5.0	1.4	8.7	83.3	136.5
24	893	25	5.3	1.6	8.8	82.6	136.5
25	905	0	5.5	1.6	8.8	87.8	135.9

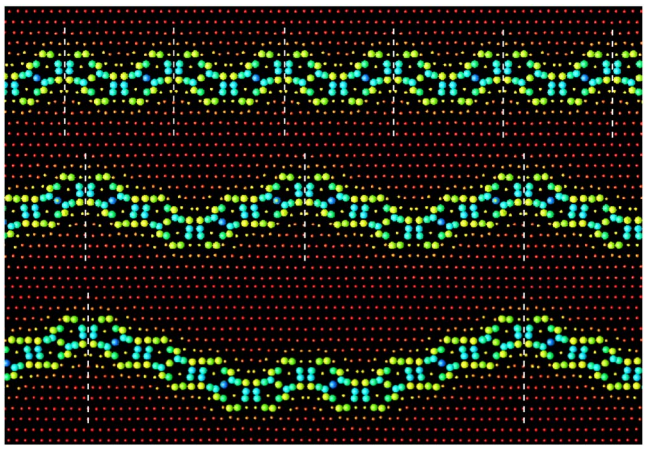

FIG. 7. (Color online) Σ13 boundaries, viewed from the side, all with 21 atoms removed per primitive cell ($\Delta N=21$). In the top figure the computational supercell comprised one primitive cell, in the middle figure it comprised 2×2 primitive cells, and in the bottom figure it comprised 4×4 primitive cells. The coloring of the atoms is an indication of the order parameter, with red marking most crystalline environments and blue least crystalline environments. The dashed lines indicate the sizes of the supercells.

energy Σ5 structure among the 1×1 primitive cell systems, which has a ΔN value of 7, is composed of the same A and B units as minimum-energy Σ13 and Σ25 boundaries (Fig. 12). This can be thought of as the limiting case of a ⟨110⟩ screw dislocation network model where the A and B units occupy alternate screw dislocation intersections. The screw dislocation intersections comprise the entire boundary plane.

We have also calculated fully relaxed structures for computational supercells comprising 2×2 primitive cells. See Table VII for detailed structural information. Here there are 40 possible ΔN values ranging from 0 to 9.75. In the 2×2 cells the boundary energies are less than or equal to the energies of the 1×1 cells with the same values of ΔN (see Fig. 13). In the case of the two lowest-energy structures for the 1×1 cells, with $\Delta N=2$ and 7, we find that the structure is identical for the 2×2 cells. The maximum energy obtained for 2×2 cells is 1292 mJ/m^2 with $\Delta N=6.25$, which is significantly lower than the 1×1 cell value of 1369 mJ/m^2 with $\Delta N=5$. We also find that there are new low-energy structures that cannot be attained with the 1×1 periodicity. The lowest-energy structure we have obtained for the Σ5 boundary is $\Delta N=8.25$ (see Fig. 14), with an energy of 1066 mJ/m^2. Despite it having an almost identical energy to $\Delta N=7$ (with second lowest energy), the structure is completely different. It has space-group symmetry $p2$, and the size of the repeat cell is 2×2 primitive cells. The structure has a row of C units, which are rotated by 45° compared to those in the Σ17 boundary. The structures with $\Delta N=8.5$ (with third lowest energy) and $\Delta N=8.75$ (with fifth lowest energy) also have a similar row of C units. Even though these are among the four lowest-energy structures, they have coordination defects and higher strain than other low-energy Σ5 structures, such as $\Delta N=7$. The structures with $\Delta N=8$ (with fourth lowest energy) and $\Delta N=9$ (with sixth lowest energy) do not show point-group symmetry. For $\Delta N=8$ there is one A unit and two B units per supercell, and for $\Delta N=9$ there are six B units per supercell. The seventh lowest-energy structure is found for $\Delta N=2$ which is identical to the one we found with a 1×1 supercell. For $\Delta N=3.5$ (with eighth lowest energy) we find a structure with no structural units, wide bond angle, and length distributions and space-group symmetry $p2_1$. The structure with $\Delta N=7.75$ (with ninth lowest energy) does not show point-group symmetry but has one C unit per supercell. $\Delta N=4$ (with tenth lowest energy) has space-group symmetry $p2_122$ and a repeat cell comprising 2×1 primitive cells. Among structures with energies higher than those listed here there are several that are partly composed of A and B units, locally recreating the $\Delta N=7$ struc-

TABLE IV. Energies in (mJ/m^2) of relaxed configurations of Σ17 for $0\leq\Delta N\leq33$ obtained with the TS potential. See caption to Table I.

ΔN	TS	W (Å)	(2,3,5,6)	σ_b (%)	σ_θ (deg)	θ_{min} (deg)	θ_{max} (deg)
0	1020	6.0	0,0,0,0	1.6	9.8	83.6	143.6
1	1096	6.2	0,0,0,0	2.0	9.8	62.8	141.9
2	1087	6.4	0,0,2,0	2.1	10.3	76.8	152.2
3	1163	6.0	0,1,1,0	2.6	11.1	62.3	159.2
4	1158	6.3	0,0,2,0	2.0	11.0	80.0	169.7
5	1158	6.3	0,0,0,0	1.7	10.0	84.5	146.2
6	1170	6.0	0,2,2,0	2.6	11.6	72.1	177.4
7	1179	6.2	0,0,2,0	2.2	11.1	81.1	171.3
8	1222	6.2	0,0,2,0	2.4	11.8	81.3	173.1
9	1193	5.7	0,0,2,0	2.4	12.1	71.9	163.6
10	1180	5.7	0,0,4,0	2.8	12.9	73.1	176.4
11	1203	5.3	0,0,6,0	2.8	14.9	73.0	179.0
12	1166	5.8	0,0,4,0	2.6	12.9	72.9	168.2
13	1173	5.9	0,2,4,0	2.3	13.6	75.8	164.7
14	1163	6.3	0,2,0,0	1.7	11.7	83.7	157.8
15	1293	7.0	0,0,4,0	2.4	12.1	70.6	168.6
16	1267	5.7	0,1,5,0	3.1	14.4	72.1	176.1
17	1274	6.9	0,4,8,0	3.1	13.9	59.0	175.0
18	1294	6.9	0,0,4,0	2.2	12.0	73.7	175.9
19	1332	7.6	0,0,6,0	2.3	12.0	71.1	177.4
20	1270	7.7	0,0,4,0	2.3	11.1	70.3	162.7
21	1200	9.1	0,0,0,0	1.6	9.3	74.6	158.7
22	1254	5.2	0,0,2,0	2.3	11.7	72.3	167.2
23	1247	5.3	0,0,2,0	2.1	12.0	71.0	161.4
24	1198	5.1	0,1,1,0	1.7	11.3	76.4	162.1
25	1149	5.2	0,2,0,0	1.5	10.4	77.9	139.0
26	1103	5.1	0,0,0,0	1.8	10.2	79.9	136.4
27	1122	5.6	0,0,0,0	1.6	10.2	77.4	144.1
28	1098	5.4	0,0,0,0	2.0	10.3	75.8	136.8
29	1097	5.4	0,0,2,0	2.3	11.2	72.8	171.9
30	1070	5.6	0,0,4,0	2.3	11.8	71.9	158.9
31	1030	5.7	0,0,2,0	2.1	11.4	77.5	158.1
32	1009	5.7	0,0,0,0	1.7	10.3	84.8	139.7
33	1037	5.8	0,2,0,0	1.7	9.9	82.9	142.5

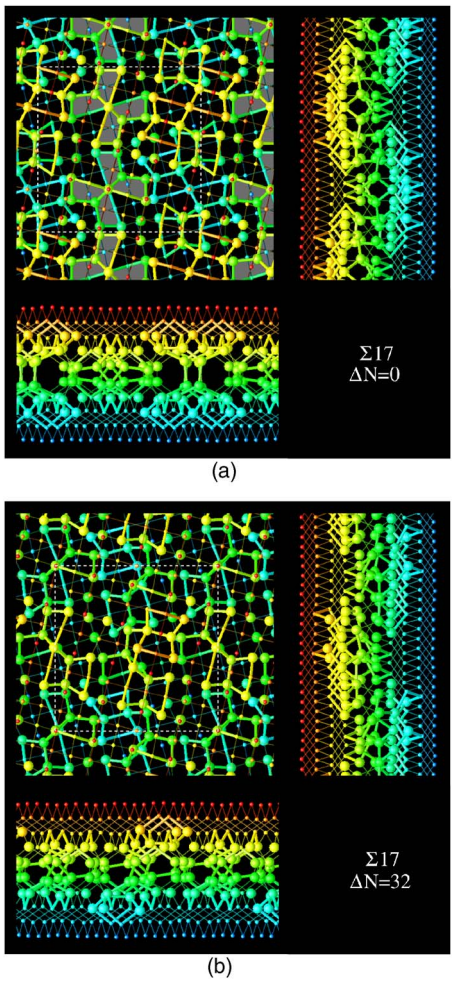

FIG. 8. (Color online) Lowest-energy Σ17 boundaries obtained with computational supercells containing one primitive cell parallel to the GB plane. See caption to Fig. 2.

ture. In the highest-energy structures there are no special structural features, such as structural units or point-group symmetry, to be seen.

The $\Delta N=7$ structure is composed of A and B units occupying alternate screw dislocation intersections. The higher-energy metastable states for $\Delta N=7$ comprising 2×2 primitive cells have several structures which are also composed of A and B units (Fig. 15). The second lowest-energy structure with $\Delta N=7$ has an energy of 1091 mJ/m^2 and is identical to the minimum-energy structure, except that one A and one B unit have exchanged places. The boundary with the fourth lowest energy has an energy of 1096 mJ/m^2 and is another arrangement of A and B units: entire rows of A and B units have exchanged places. Finally the boundary for $\Delta N=7$ with the tenth lowest energy, 1121 mJ/m^2, is the same as the minimum-energy state except two A and B units have exchanged places. The other metastable states did not contain complete A and B units.

E. Σ29 boundary

The Σ29 boundary has a misorientation of approximately 44° which is the largest studied here. In each primitive cell in the GB plane there are 29 atoms per layer giving 58 possible values of ΔN. In Table VIII we have given structural information for the supercells containing one primitive cell in the GB plane. The difference in energy and strain between the high- and low-energy structures is smaller than for other boundaries. The lowest-energy structures are higher in energy than for other boundaries, while the high-energy structures are similar to the high-energy structures of other boundaries in terms of the energy, bond angle distributions, bond length distributions, and the absence of point-group symmetry.

The minimum-energy structure has $\Delta N=47$ and an energy of 1108 mJ/m^2. There are two fivefold-coordinated atoms per primitive cell. It has a wider bond angle distribution than

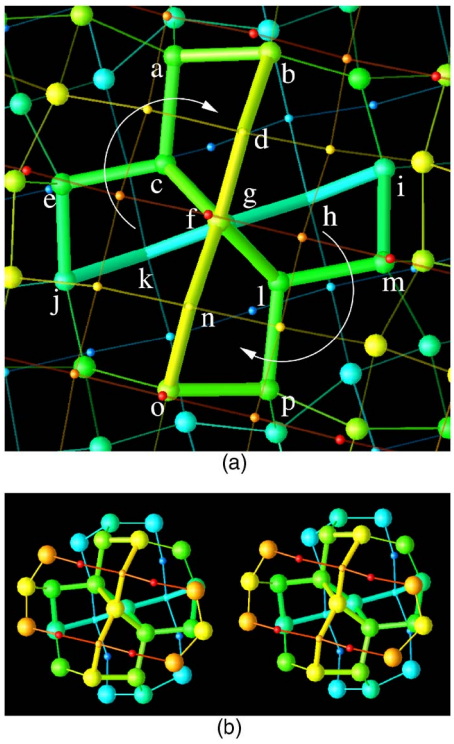

FIG. 9. (Color online) The C structural unit. Upper figure: atoms in five-membered rings are labeled (see text), and arrows indicate the sense of the spirals formed by the five-membered rings. Lower figure: stereo image. See caption to Fig. 2.

TABLE V. Energies (mJ/m^2) of relaxed configurations of Σ17 with 2×2 primitive cells obtained with the TS potential. See caption to Table I.

ΔN	TS	W (Å)	(2,3,5,6)	σ_b (%)	σ_θ (deg)	θ_{min} (deg)	θ_{max} (deg)
0	1036	6.3	0,2,4,0	2.1	9.7	75.1	158.3
31	1017	5.9	0,1,7,0	2.0	10.6	73.9	170.9
31.5	1007	5.8	0,0,6,0	2.1	10.5	69.8	167.6
32	1038	5.9	0,0,8,0	2.1	11.2	72.9	174.8
32.5	1007	6.3	0,0,6,0	2.0	9.9	72.5	159.4
33	1048	6.2	0,2,2,0	1.9	9.9	71.7	171.8
33.5	1027	6.1	0,0,4,0	2.0	9.9	72.8	170.0

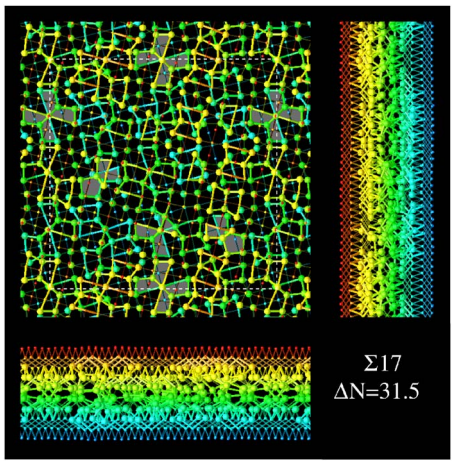

FIG. 10. (Color online) Σ17 boundary with $\Delta N=31.5$ where each simulation supercell comprised 2×2 primitive cells in the GB plane. The *C* unit has been marked in the same fashion as *A* and *B* units. See caption to Fig. 2.

the minimum-energy structures of other boundaries studied here. A network of $\frac{1}{2}\langle110\rangle$ screw dislocations cannot be distinguished but there are *B* units visible in the plan view (Fig. 16). The boundary possesses space-group symmetry *p*2. However, there are indications that this is not the minimum-energy structure. We have carried out several quenches for $\Delta N=47$, and only one quench gave the minimum-energy structure we have presented. This suggests that for Σ29 there is no clear minimum-energy structure with small strain and small energy. But it is also possible that for the Σ29 boundary, having the largest primitive cell area and misorientation considered here, much longer quenches are required to find the true minimum-energy state. In addition, removing the constraint of having only one primitive cell in the GB plane might allow the boundary to find a more ordered structure.

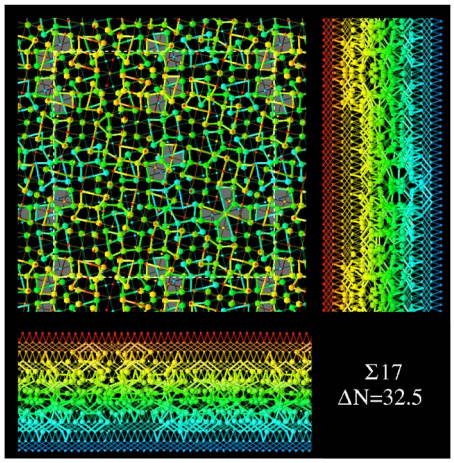

FIG. 11. (Color online) Σ17 boundary with $\Delta N=32.5$ where each simulation supercell comprised 2×2 primitive cells in the GB plane. The *C* unit has been marked in the same fashion as *A* and *B* units. See caption to Fig. 2.

TABLE VI. Energies (mJ/m^2) of relaxed configurations of Σ5 for $0\leq\Delta N\leq9$ obtained with the TS potential. See caption to Table I.

ΔN	TS	W (Å)	(2,3,5,6)	σ_b (%)	σ_θ (deg)	θ_{min} (deg)	θ_{max} (deg)
0	1244	6.7	0,0,2,0	3.5	12.7	70.7	157.4
1	1295	7.2	0,0,2,0	2.4	12.6	73.6	169.2
2	1104	7.4	0,0,0,0	1.7	9.2	92.1	138.6
3	1189	5.4	0,0,4,0	2.7	16.2	73.6	169.2
4	1232	4.2	0,0,2,0	2.8	17.8	76.8	175.8
5	1369	4.8	0,4,0,0	3.0	17.4	74.3	173.2
6	1312	6.2	0,0,2,0	2.1	13.3	74.6	159.7
7	1070	5.9	0,0,0,0	1.4	9.4	85.0	134.7
8	1267	6.3	0,0,4,0	3.0	15.7	58.3	153.8
9	1169	3.9	0,0,0,0	2.3	14.4	81.5	143.9

IV. DISCUSSION

A. Dependence of structure on $\Delta N/\nu$

By considering a primitive cell of a (001) twist boundary in Si we have seen that distinct structures may be obtained by removing ΔN atoms from each primitive cell, where $0\leq\Delta N<2\nu$ and ν depends on the boundary misorientation. When $\Delta N=2\nu$ we remove two entire (004) layers, which regenerates the boundary structure with $\Delta N=0$. Thus, at each misorientation the boundary energy is a periodic function of $\Delta N/\nu$ with a periodicity of 2. The energies of boundaries for all five misorientations studied here are plotted in Fig. 17 as a function of $\Delta N/\nu$ for $0\leq\Delta N\leq2\nu$. For each boundary the energy sweeps through a range of values as $\Delta N/\nu$ varies between 0 and 2. As the boundary misorientation increases the variation of its energy with $\Delta N/\nu$ decreases. The variation of the energy with $\Delta N/\nu$ is a measure of the extent to which the structure resists perturbation. If the boundary structure were liquid like or amorphous, we would expect the boundary energy to be independent of $\Delta N/\nu$.That the boundary energy varies by 17% even for Σ29 indicates that none of

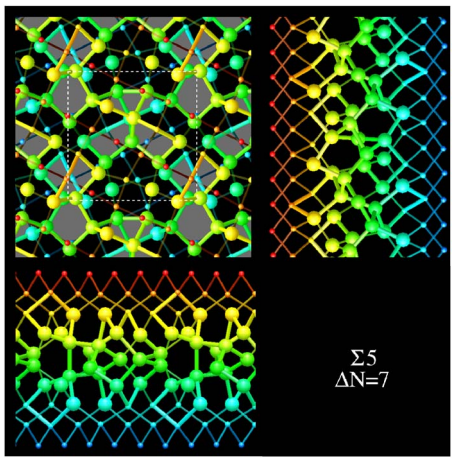

FIG. 12. (Color online) The lowest-energy Σ5 boundary with a computational cell of 1×1 primitive cells. See caption to Fig. 2.

TABLE VII. Energies (mJ/m^2) of relaxed configurations of $\Sigma 5$ with 2×2 primitive cells for $0 \leq \Delta N \leq 9.75$ obtained with the TS potentials. See caption to Table I.

ΔN	TS	W (Å)	(2,3,5,6)	σ_b (%)	σ_θ (deg)	θ_{min} (deg)	θ_{max} (deg)
0	1174	7.6	0,0,2,0	2.2	10.0	70.1	157.4
0.25	1238	6.8	0,0,2,0	2.3	10.8	76.3	175.6
0.5	1206	7.3	0,1,1,0	2.2	9.8	72.5	158.4
1	1178	7.2	0,2,0,0	1.9	8.9	81.8	142.2
1.25	1161	7.7	0,1,1,0	2.0	9.2	79.8	155.7
1.5	1240	6.8	0,0,2,0	2.3	11.0	70.6	166.1
1.75	1131	7.3	0,0,0,0	1.8	9.0	78.0	141.2
2	1104	7.4	0,0,0,0	1.7	9.2	92.1	138.6
2.25	1232	6.5	0,0,6,0	2.5	12.6	56.3	169.2
2.5	1229	6.3	0,2,2,0	2.3	11.3	64.3	169.2
2.75	1193	5.5	0,0,2,0	2.3	12.1	82.2	170.9
3	1178	6.4	0,0,10,0	2.7	13.7	58.7	169.3
3.25	1160	5.3	0,0,6,0	2.7	13.6	73.0	169.8
3.5	1113	5.5	0,0,4,0	2.6	12.5	79.8	168.3
3.75	1140	5.1	0,2,4,0	2.8	13.4	78.6	170.5
4	1117	7.2	0,0,0,0	1.3	10.2	88.2	133.6
4.25	1180	6.2	0,2,2,0	2.2	11.7	76.8	169.1
4.5	1182	7.3	0,0,0,0	1.6	9.9	86.5	143.3
4.75	1239	6.0	0,1,5,0	3.0	13.0	75.8	173.1
5	1216	5.9	0,2,4,0	2.6	12.3	76.9	171.5
5.25	1289	7.7	0,0,4,0	2.1	11.7	74.0	178.0
5.5	1277	6.8	0,0,2,0	2.3	10.9	73.2	164.3
5.75	1281	6.6	0,2,2,0	2.4	11.1	70.8	173.5
6	1218	7.6	0,0,4,0	2.0	10.8	71.3	167.6
6.25	1292	8.2	0,0,2,0	2.1	10.0	73.8	173.2
6.5	1250	7.8	0,1,3,0	2.0	10.5	77.2	173.6
6.75	1130	6.0	0,0,2,0	1.6	10.5	75.1	158.3
7	1070	5.9	0,0,0,0	1.4	9.4	85.0	134.6
7.25	1120	6.2	0,1,1,0	1.9	10.1	76.8	171.8
7.5	1120	6.2	0,1,1,0	1.9	10.1	70.6	162.3
7.75	1116	6.7	0,1,3,0	2.2	11.0	71.1	172.3
8.0	1088	6.5	0,0,2,0	2.1	10.5	71.4	171.9
8.25	1066	7.2	0,0,2,0	2.0	10.3	81.1	169.7
8.5	1070	6.8	0,0,8,0	2.4	12.2	72.1	165.6
8.75	1088	7.1	0,0,6,0	2.6	11.5	69.7	168.0
9	1094	7.3	0,0,0,0	1.7	8.6	85.3	139.4
9.25	1131	7.6	0,0,0,0	1.8	9.1	83.2	136.3
9.5	1141	7.5	0,0,0,0	1.8	9.1	82.8	144.1
9.75	1176	6.8	0,0,2,0	2.1	10.6	77.3	160.7

the boundary misorientations may be regarded as having a liquidlike or amorphous structure.

In Fig. 17 we have drawn solid lines for each boundary misorientation. But for any periodically repeated supercell, $\Delta N/\nu$ may assume only certain discrete values. In Fig. 17 the supercells comprise 1×1 primitive cells. The solid lines connecting the discrete points are merely to guide the eye.

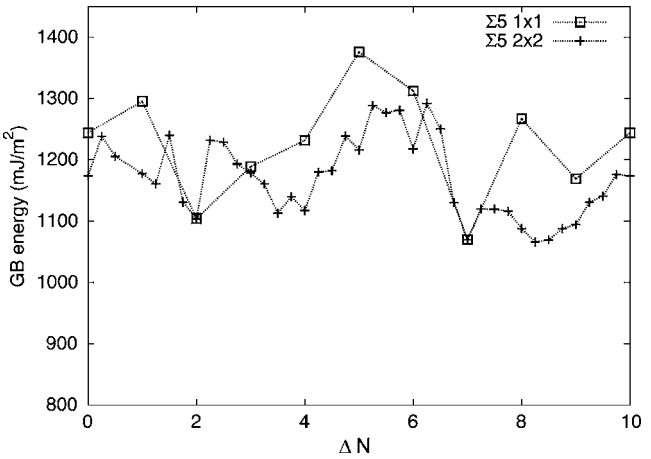

FIG. 13. $\Sigma 5$ GB energies obtained with the TS potential as a function of the number ΔN of atoms removed per primitive cell in 1×1 and 2×2 supercells. Lines between data points are only to guide the eye.

This raises the question of whether the boundary energy may be depicted in principle as a continuous function of $\Delta N/\nu$. We present an argument in favor of this proposition, based on the following thought experiment. At a given misorientation we carry out simulations for computational supercells comprising $N_p \times N_p$ primitive cells, where $N_p = 1, 2, 3, \ldots, \infty$. By choosing N_p sufficiently large we will always be able to create a boundary structure with any required value of $\Delta N/\nu$. The lowest energy attained for this value of $\Delta N/\nu$ may then be plotted on a graph like those shown in Fig. 17. In this way the boundary energy may be defined as a continuous function of $\Delta N/\nu$ and plotted as in Fig. 17. We note that there may be higher-energy metastable states than those shown in Fig. 17 at each value of $\Delta N/\nu$.

A graph of GB energy against $\Delta N/\nu$ enables us to evaluate the efficiency of the boundary as a source or sink of vacancies at 0 K. For each value of $\Delta N/\nu$ the slope of the graph indicates whether the boundary energy changes on emitting or adsorbing a vacancy. Only if the energy is independent of $\Delta N/\nu$ is the boundary a perfect source or sink for

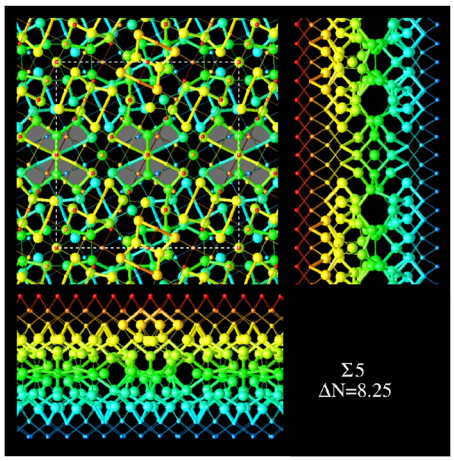

FIG. 14. (Color online) The lowest-energy $\Sigma 5$ boundary with a computational cell of 2×2 primitive cells. See caption to Fig. 2.

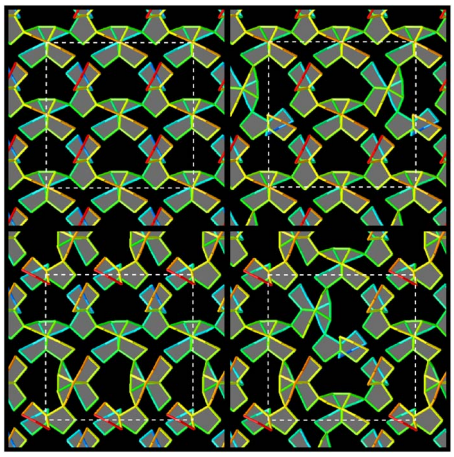

FIG. 15. (Color online) Σ5 boundaries where each computational supercell contained $2\times2=4$ primitive cells in the GB plane. In each case the number of atoms removed per primitive cell is $\Delta N=7$. The boundary energies are 1069, 1091, 1095, and 1121 mJ/m^2 for the top left, top right, bottom left, and bottom right configurations, respectively. The size of the 2×2 supercell is indicated by a white dashed box. Bonds in only five-membered rings are shown to highlight the structural units. See caption to Fig. 2.

vacancies. We have also noted that the boundary structure may be very sensitive to the number of atoms removed per unit area. By removing one atom per primitive cell from the Σ5 boundary with $\Delta N=7$ and 2×2 primitive cells we found a completely new structure. This suggests that in absorbing or emitting a vacancy in each primitive cell the point defect may become delocalized and lead to a restructuring of the boundary.

B. Dependence of GB structure on the size of a supercell

In addition to supercells comprising one primitive cell we have also calculated larger supercells comprising 2×2 primitive cells for Σ13, Σ17, and Σ5 boundaries. Owing to computational constraints we carried out a complete survey of all possible ΔN values only for the Σ5 boundary.

In the case of nonprimitive supercells it is possible to find repeat cells comprising 1×1, 1×2, 2×1, $\sqrt{2}\times\sqrt{2}$, $2\times2,\ldots$ primitive cells. The energy of a larger supercell should always be smaller than, or equal to, the energy of a 1×1 supercell with the same value of ΔN. We found that for the Σ5 boundary this expectation was satisfied at all values of ΔN accessible to the 1×1 structure, while for Σ13 and Σ17 boundaries our quenches were not always sufficient to find the minimum-energy structure for larger supercells. For each boundary we found structures with larger repeat cells which lowered the energy compared with the repeat cells comprising one primitive cell. Nevertheless, for all boundaries there were very small energy differences between the lowest-energy structures obtained with the 1×1 supercells cells and those obtained with larger supercells.

It is clear that one needs to consider nonprimitive supercells to access the full range of boundary structures even at absolute zero. It becomes increasingly difficult to locate global minimum-energy structures as the size of the supercell

TABLE VIII. Energies in (mJ/m^2) of relaxed configurations of Σ29 for $0\leq\Delta N\leq58$ obtained with the TS potential. See caption to Table I.

ΔN	TS	W (Å)	(3,5)	σ_b (%)	σ_θ (deg)	θ_{min} (deg)	θ_{max} (deg)
0	1259	6.8	0,0,4,0	2.4	11.1	72.5	170.9
1	1229	6.8	0,0,4,0	2.3	11.2	74.0	172.6
2	1266	7.0	0,1,5,0	2.7	11.4	59.4	155.1
3	1261	7.2	0,0,2,0	2.1	10.2	77.4	148.4
4	1227	6.8	0,0,4,0	2.2	11.3	77.2	168.8
5	1239	6.6	0,1,1,0	2.1	10.5	76.3	164.2
6	1283	7.1	0,1,11,0	2.7	12.7	61.9	172.2
7	1292	6.9	0,0,2,0	2.1	10.8	76.1	165.0
8	1290	7.3	0,0,4,0	2.1	11.0	71.9	166.1
9	1277	7.9	0,0,6,0	2.0	11.1	73.3	170.2
10	1311	7.4	0,0,4,0	2.1	10.7	72.2	160.7
11	1295	7.2	0,0,10,1	2.3	13.0	58.4	171.2
12	1271	7.3	0,0,8,0	2.3	11.8	56.8	164.8
13	1250	7.1	0,2,2,0	2.2	10.3	71.8	159.2
14	1231	6.4	0,1,7,0	2.1	12.2	72.3	172.1
15	1227	6.5	0,1,5,0	2.3	12.0	72.8	164.7
16	1144	6.4	0,0,6,0	2.3	11.5	61.9	171.6
17	1165	6.9	0,0,6,0	2.0	11.5	72.5	166.7
18	1156	7.4	0,1,5,0	2.0	10.9	73.0	165.7
19	1170	6.9	0,1,5,0	2.1	11.0	63.0	170.3
20	1137	7.1	0,1,5,0	2.0	10.9	72.0	167.3
21	1155	6.5	0,0,4,0	2.3	11.0	71.0	169.7
22	1136	6.8	0,0,6,0	2.4	11.6	60.6	167.7
23	1175	7.0	0,1,9,0	2.6	11.9	57.2	168.1
24	1187	6.3	0,0,0,0	2.0	10.6	81.2	151.5
25	1279	6.7	0,1,3,0	2.1	11.5	74.2	165.6
26	1193	7.3	0,3,5,0	2.1	10.6	72.3	170.2
27	1229	6.7	0,2,0,0	1.9	10.2	78.1	161.1
28	1274	6.1	0,0,2,0	2.5	11.3	72.3	163.6
29	1264	7.4	0,1,3,0	2.1	10.5	71.6	165.1
30	1252	7.1	0,1,3,0	2.1	10.2	74.1	168.8
31	1250	7.7	0,0,10,0	2.6	11.5	57.3	168.5
32	1260	7.2	0,1,5,0	2.2	11.2	62.7	173.7
33	1289	6.9	0,1,5,0	2.5	11.0	59.2	157.7
34	1300	6.5	0,0,8,0	2.5	12.6	70.8	171.5
35	1332	7.7	0,4,2,0	2.0	10.5	77.3	165.7
36	1314	7.7	0,0,2,0	2.1	10.5	59.7	155.5
37	1258	6.6	0,0,4,0	2.0	11.2	75.0	168.7
38	1289	7.1	0,0,14,0	2.8	13.2	57.4	168.8
39	1310	7.5	0,1,7,0	2.2	11.4	72.3	178.3
40	1237	7.1	0,1,3,0	2.3	10.7	58.0	165.3
41	1243	6.8	0,1,5,0	2.1	11.0	58.9	156.4
42	1237	6.9	0,0,6,0	2.1	11.8	58.0	171.0
43	1231	7.0	0,0,6,0	2.4	11.6	63.7	165.0
44	1240	6.6	0,2,4,0	2.2	11.2	72.7	158.8
45	1195	6.9	0,0,4,0	1.9	11.1	73.9	171.6

TABLE VIII. (*Continued.*)

ΔN	TS	W (Å)	(3,5)	σ_b (%)	σ_θ (deg)	θ_{min} (deg)	θ_{max} (deg)
46	1170	6.3	0,1,5,0	2.0	11.3	72.8	165.4
47	1108	6.4	0,0,2,0	1.8	10.1	79.2	164.5
48	1155	6.2	0,0,4,0	2.3	11.2	72.7	167.7
49	1143	6.6	0,2,2,0	2.1	10.5	79.4	169.6
50	1175	6.8	0,0,4,0	2.0	11.2	72.3	165.4
51	1187	6.9	0,2,6,0	2.3	11.6	72.1	172.8
52	1180	5.9	0,1,5,0	2.6	12.2	71.3	170.8
53	1208	6.0	0,2,4,0	2.6	11.9	60.9	169.8
54	1208	6.7	0,1,3,0	2.3	11.1	71.6	169.0
55	1229	6.5	0,1,3,0	2.1	11.2	74.1	173.1
56	1249	7.0	0,1,3,0	2.2	10.9	73.3	169.7
57	1237	6.7	0,0,4,0	2.3	11.2	73.5	172.6

~increases because the number of degrees of freedom increases. In addition the number of possible values of ΔN increases as the size of the supercell increases. By using smaller supercells it is easier to study all possible values of ΔN and have more confidence in finding global minimum-energy states. These structures are a good starting point for considering larger boundaries.

C. Structural order

We found that independent simulations of $\Sigma 25$, $\Sigma 13$, $\Sigma 17$, and $\Sigma 5$ boundaries comprising one primitive cell, with values of ΔN corresponding to low-energy structures, converged in each case to the same minimum-energy structure. This provides some confidence that for these boundaries we have found structures with the lowest possible energy. In addition to the periodicity imposed within the boundary plane there is further structural order displayed in these boundaries. On the other hand, for the $\Sigma 29$ boundary and

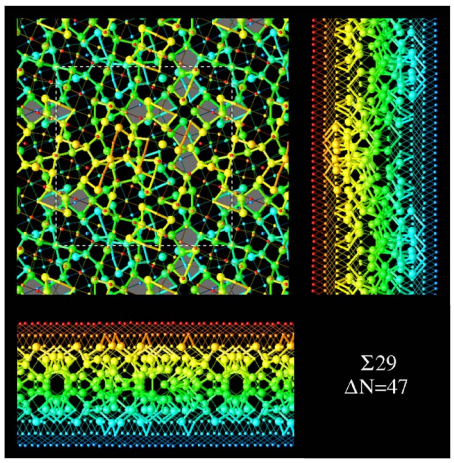

FIG. 16. (Color online) Lowest-energy $\Sigma 29$ boundary obtained with a supercell of one primitive cell in the GB plane. See caption to Fig. 2.

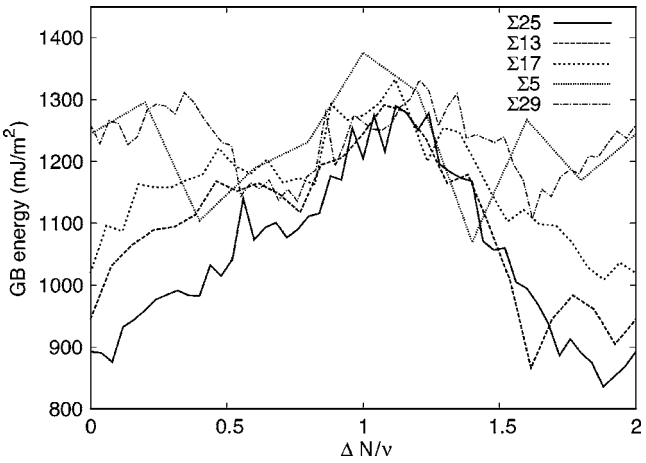

FIG. 17. GB energy obtained with the TS potential as a function of the number ΔN of atoms removed normalized by the number ν of atoms in each layer parallel to the GB contained in one primitive cell of the GB.

$\Sigma 13$, $\Sigma 17$, and $\Sigma 5$ boundaries comprising 2×2 primitive cells we did not always obtain the same structures in independent simulations. This is an indication of the difficulty in finding the minimum-energy structure of larger supercells. The structures in these boundaries appear less ordered. But even these structures cannot be described as an amorphous film because they all exhibit point-group symmetry, with the exception of the $\Sigma 17$ boundary. The $\Sigma 17$ boundary comprising 2×2 primitive cells does show some degree of order since it displays characteristic structural units found also in other boundaries.

The GB structures comprising one primitive cell are less distorted than amorphous silicon. Using the TS potential with a 20-ns quench from the melt we find $\sigma_\theta = 11^\circ$ and $\sigma_b = 2.2\%$ for amorphous Si. For the minimum-energy structures of $\Sigma 25$, $\Sigma 13$, $\Sigma 17$, and $\Sigma 5$ boundaries we find that $\sigma_\theta = 9.1^\circ - 9.5^\circ$ and that $\sigma_b = 1.4\% - 1.6\%$. For the minimum-energy structure of the $\Sigma 29$ boundary we find that $\sigma_\theta = 10.1^\circ$ and $\sigma_b = 1.8\%$ which is higher than for the other boundaries but still smaller than the values for amorphous Si. Also the maximum strain is smaller in the low-energy structures which is evident from the maximum- and minimum-bond-angle values. We also see that, with the exception of $\Sigma 29$ boundaries, the minimum-energy structures do not contain bonding defects. For the high-energy configurations of $\Sigma 25$, $\Sigma 13$, $\Sigma 17$, $\Sigma 5$, and $\Sigma 29$ boundaries we find that the value of σ_θ and σ_b are close to the amorphous values and that these boundaries also contain bonding defects. These correlations between boundary energy, on the one hand, and coordination defects and bond length and angle distortions, on the other hand, are a clear signature of local order in the low-energy configurations.

Another geometrical argument for order is that there are point-group symmetries present in all minimum-energy configurations. The minimum-energy structures of $\Sigma 25$, $\Sigma 13$, $\Sigma 17$, $\Sigma 5$, and $\Sigma 29$ have space group $p2$, $p2_122$, $p2_1$, $p2$, and $p2$, respectively. In addition there are several other low-energy structures which show symmetry; e.g., $\Sigma 17$ with $\Delta N = 0$ have space group $p2_122$ and $\Sigma 5$ with $\Delta N = 2, 9$ have

TABLE IX. Minimum relaxed energies (E) in mJ/m^2 of $\Sigma 25$, $\Sigma 13$, $\Sigma 17$, $\Sigma 5$, and $\Sigma 29$ boundaries with 1×1 simulation cells obtained with the TS potential. Also given are the changes in energy in eV per 1×1 cell when an atom is added to each 1×1 cell ($\Delta E_{\Delta N-1}$) or an atom is removed ($\Delta E_{\Delta N+1}$). ΔE is the energy difference in eV per 1×1 cell to the second lowest-energy structure for the same ΔN. Finally the space group to which each boundary belongs is given.

Σ	ϕ	E	$\Delta E_{\Delta N-1}$	$\Delta E_{\Delta N+1}$	ΔE	Space group
25	16	836	0.89	0.37	0.37	$p2$
13	23	866	1.69	0.93	0.77	$p2_122$
17	28	1009	0.32	0.43	0.17	$p2_1$
5	37	1070	1.12	0.91	0.32	$p2$
29	44	1108	1.67	1.26	0.20	$p2$

space groups $p222$ and $p2_122$, respectively. Such point-group symmetries are incompatible with structural disorder. We also note that $\Sigma 25$, $\Sigma 13$, and $\Sigma 5$ boundaries contain the same structural units which shows that their structures are not arbitrary or disordered.

There are significant energy costs associated with adding or removing atoms from the lowest-energy structures comprising one primitive cell, as seen in Table IX. In our simulations we find a number of metastable structures all sharing the same value of ΔN. Table IX also shows the energy difference between the minimum-energy structure and the next-lowest-energy configuration for the same value of ΔN. These are further indications that the minimum-energy structures comprising one primitive cell resist perturbation and they are not disordered.

It is evident that the $\Sigma 25$, $\Sigma 13$, $\Sigma 17$, and $\Sigma 5$ boundaries comprising one primitive cell are ordered according to all criteria discussed here. The case of $\Sigma 29$ is not as clear; the structure has more defects, larger bond angle, and bond length deviations than the other minimum-energy structures. Nevertheless, the point-group symmetry found in the minimum-energy configuration of even this boundary is a clear indication that it cannot be described as amorphous or disordered.

D. Structural unit model

We have seen that those twist grain boundaries in which the network of $\frac{1}{2}\langle 110\rangle$ screw dislocations is clearly visible—i.e., $\Sigma 25$, $\Sigma 13$, and $\Sigma 5$ boundaries—are composed of clearly identifiable structural units. We have identified two structural units, *A* and *B* for the screw dislocation intersections (Figs. 3 and 4). The core structures of the screw dislocations were shown to be composed of dimer configurations, located in the upper and lower grains. In the $\Sigma 25$ structure there are two and in the $\Sigma 13$ structure there is one dimer between each intersection. In the $\Sigma 5$ structure the structural units at the screw dislocation intersections are so close to each other that they touch (Fig. 12). The minimum-energy state of both $\Sigma 25$ and $\Sigma 5$ boundaries is for the intersections to be occupied alternately by *A* or *B* units.

For the $\Sigma 13$ boundary we have found that one can form ordered networks containing different mixes of *A* and *B* units (Fig. 6). Structures containing both *A* and *B* units are found only after quenching computational supercells comprising more than one primitive cell in the GB plane. In the case of one primitive cell one could theoretically have a structure with one *A* and one *B* unit but it does not seem to be stable since we have not found it. In supercells comprising 2×2 primitive cells with $\Delta N=21$, 22, 23, 24, and 25, we found 100%, 75%, 50%, 25%, and 0% of the screw dislocation intersections to be *A* units, respectively. The rest of the intersections were *B* units. The energies of these structures were 858, 869, 876, 893, and 905 mJ/m^2, respectively. The energy increases roughly linearly with the fraction of *B* units in the boundary. It is reasonable to presume that even larger $\Sigma 13$ boundaries can be constructed using the same structural units as building blocks.

For the $\Sigma 5$ boundary there are configurations which differ in the packing of *A* and *B* units. In a supercell comprising 2×2 primitive cells we found for $\Delta N=7$ that there are several ways of packing *A* and *B* units, one of which is the ground state (Fig. 15). For $\Delta N\neq 7$ we did not find structures composed of *A* and *B* units even in nonprimitive supercells. In this high-angle boundary it seems that it is unfavorable to have any fraction of *A* and *B* other than 50% even though one can vary the packing pattern of the *A* and *B* units with a relatively small energy penalty. In the case of $\Sigma 25$ we have not performed simulations with nonprimitive supercells but the small misorientation leads us to conjecture that this boundary will be able to adopt configurations with a different fraction of *A* and *B* units. In fact we have found one structure ($\Delta N=43$) where the boundary consists of *A* units only.

E. Comparison to previous results

To make a direct comparison with an earlier published result we have also relaxed our structures further using the SW potential. With this our lowest-energy structure for the $\Sigma 17$ (001) twist boundary in Si is obtained with $\Delta N=0$ and is 1027 mJ/m^2. For $\Delta N=32$, which was the minimum-energy structure in the case of the TS potential, the GB energy using SW potential is 1040 mJ/m^2. This is 25% lower than the value of 1370 mJ/m^2 obtained in Ref. 6, where the quench was two orders of magnitude shorter in duration. Our lowest-energy structure obtained with the SW potential for the $\Sigma 5$ boundary is for the $\Delta N=2$ configuration, with an energy of 1049 mJ/m^2. For $\Sigma 29$ we obtained a GB energy of 1109 mJ/m^2 with $\Delta N=47$. We believe that these energies are significantly lower than any energies obtained before for these boundaries with the SW potential. Thus we can conclude that not only do we find the boundaries to be ordered; we have also found significantly lower-energy configurations.

We note that it has previously been shown that allowing the number of atoms at twist grain boundaries to vary is crucially important in rocksalt structured ionic oxides.[19] In this case the removal of one or more ions allows close pairings of like-charged ions across the interface to be avoided, which lowers the boundary energy dramatically.

V. CONCLUSIONS

In this paper we have studied structures of the Σ25, Σ13, Σ17, Σ5, and Σ29 (001) twist grain boundaries in Si at absolute zero. Our structures show remarkable characteristics in several ways. For each GB the energy and structure vary with the value of ΔN. By considering all values of ΔN for a primitive cell we have accessed new configurations, some of which are significantly lower in energy than those generated before. The GB energy increases with the amount of distortion of bond lengths and angles and with the number of coordination defects. The lowest-energy boundaries have no coordination defects, and the bond angle and bond length distributions are narrower than in amorphous Si. Also worth noting is that $\Delta N=0$ and ν, which are the only configurations considered by previous workers, are not the lowest-energy states for any of the boundaries. We addressed the question of structural order at an interface both geometrically and physically. We found *ordered* configurations for Σ25, Σ13, Σ17, and Σ5 at 0 K, consistent with experimentally observed energy cusps at these misorientations.[7] Further we found evidence that the structural unit model is also applicable in some twist GB's, with low-energy Σ25, Σ13, and Σ5 configurations composed of the same basic structural units. Although we find that Σ29 has the highest energy of all boundaries we have studied, in agreement with Ref. 7, we find that even this boundary displays structural order such as faceting and point-group symmetry.

Our results indicate that earlier simulations[5,6,9–13] of this and most likely other twist boundaries in covalent semiconductors have failed to locate the global energy minima. There are two principal reasons. First, only $\Delta N=0$ and ν were considered prior to this work. Some authors[10] have noted that this restriction may be a serious limitation, but presumably for reasons of limited computing resources were unable to remove it. Second, MD quenches from the melt are required to be at least tens of nanoseconds in duration to sample adequately the configurational phase space, such as the propensity for the GB to facet. Earlier simulations to obtain ground-state configurations of twist, asymmetric tilt, and mixed tilt and twist boundaries in Si should now be reassessed in the light of these findings. It is clear that locating global energy minima of twist boundaries in covalent materials requires computational resources that were not widely available as recently as a decade ago.

ACKNOWLEDGMENTS

S.v.A. and K.K. acknowledge the support of the Academy of Finland under the Finnish Centre of Excellence Programme 2006- 2011 (Project No. 123470, Computational Complex Systems Research). A.P.S. acknowledges the financial support of the European Commission under Contract No. NMP3-CT-2005-013862 (INCEMS).

[1] C. D'Anterroches and A. Bourret, Philos. Mag. A **49**, 783 (1984).
[2] M. Kohyama, R. Yamamoto, Y. Ebata, and M. Kinoshita, J. Phys. C **21**, 3205 (1988).
[3] A. Sutton, in *Polycrystalline Seiconductors II, Springer Proceedings in Physics*, edited by J. Werner and H. Strunk (Springer-Verlag, Berlin, 1991), p. 116.
[4] A. P. Sutton and V. Vitek, Philos. Trans. R. Soc. London, Ser. A **309**, 1 (1983).
[5] P. Keblinski, S. R. Phillpot, D. Wolf, and H. Gleiter, Phys. Rev. Lett. **77**, 2965 (1996).
[6] P. Keblinski, S. R. Phillpot, and D. Wolf, J. Am. Ceram. Soc. **80**, 177 (1997).
[7] A. Otsuki, Interface Sci. **9**, 293 (2001).
[8] S. von Alfthan, P. D. Haynes, K. Kaski, and A P. Sutton, Phys. Rev. Lett. **96**, 055505 (2006).
[9] F. Cleri, P. Keblinski, L. Colombo, S. R. Phillpot, and D. Wolf, Phys. Rev. B **57**, 6247 (1998).
[10] E. Tarnow, P. Dallot, P. D. Bristowe, J. D. Joannopoulos, G. P. Francis, and M. C. Payne, Phys. Rev. B **42**, 3644 (1990).
[11] M. C. Payne, P. D. Bristowe, and J. D. Joannopoulos, Phys. Rev. Lett. **58**, 1348 (1987).
[12] M. Kohyama and R. Yamamoto, Phys. Rev. B **49**, 17102 (1994).
[13] Z. Q. Wang, S. A. Dregia, and D. Stroud, Phys. Rev. B **49**, 8206 (1994).
[14] J. Tersoff, Phys. Rev. B **38**, 9902 (1988).
[15] M. P. Allen and D. J. Tildesley, *Computer Simulation of Liquids* (Oxford University Press, Oxford, 1989).
[16] H. J. C. Berendsen, J. P. M. Postma, W. F. van Gunsteren, A. DiNola, and J. R. Haak, J. Chem. Phys. **81**, 3684 (1984).
[17] F. H. Stillinger and T. A. Weber, Phys. Rev. B **31**, 5262 (1985).
[18] P. R. ten Wolde, M. J. Ruiz-Montero, and D. Frenkel, Phys. Rev. Lett. **75**, 2714 (1995).
[19] P. W. Tasker and D. M. Duffy, Philos. Mag. A **47**, L45 (1983).